Excimer Laser Production, Assembly, Sintering, and Fragmentation of Novel Fullerene-like Permalloy Particles in Liquid

ARTICLE *in* THE JOURNAL OF PHYSICAL CHEMISTRY C · MARCH 2010

Impact Factor: 4.77 · DOI: 10.1021/jp911566a

8 AUTHORS, INCLUDING:

Zijie Yan
Clarkson University
41 PUBLICATIONS **498** CITATIONS
SEE PROFILE

A. N. Caruso
University of Missouri - Kansas City
62 PUBLICATIONS **685** CITATIONS
SEE PROFILE

D. B. Chrisey
Tulane University
454 PUBLICATIONS **10,578** CITATIONS
SEE PROFILE

Excimer Laser Production, Assembly, Sintering, and Fragmentation of Novel Fullerene-like Permalloy Particles in Liquid

Zijie Yan,[†] Ruqiang Bao,[†] Yong Huang,[‡] A. N. Caruso,[§] Syed B. Qadri,[||] Cerasela Zoica Dinu,*[,⊥] and Douglas B. Chrisey*[,†]

Department of Materials Science and Engineering, Rensselaer Polytechnic Institute, Troy, New York 12180, Department of Mechanical Engineering, Clemson University, Clemson, South Carolina 29634, Department of Physics, University of Missouri-Kansas City, Kansas City, Missouri 64110, U.S. Naval Research Laboratory, Washington, D.C. 20375, and Department of Chemical Engineering, West Virginia University, Morgantown, West Virginia 26506

Received: December 6, 2009

We report the fabrication of permalloy nanoparticles by pulsed excimer laser ablation of a permalloy ($Fe_{19}Ni_{81}$) target in sodium dodecyl sulfate aqueous solution and the subsequent laser-induced assembly, sintering, and fragmentation of the nanoparticles. Specifically, permalloy nanoparticles with diameters of 400−600 nm were observed to assemble into fullerene-like hollow microparticles. Laser irradiation caused sintering of the assembled particles, which showed Wulff construction and ledge growth behavior and finally resulted in smooth shells. Laser−particle interactions also caused fragmentation of the micro/nanoparticles. When the particle concentration is high, laser fragmentation rather than laser ablation dominates due to enhanced light absorption and scattering. The experiments reveal the dynamic process of the nano- and microparticle formation, demonstrating the rich processing environment of laser ablation in liquid.

1. Introduction

Fabrication of nanoparticles by laser ablation of bulk materials in liquid has attracted interest as an alternative approach to traditional chemical methods.[1−5] By optimizing the laser parameters (e.g., wavelength, pulse width, fluence, and repetition frequency) and using an appropriate liquid medium (e.g., aqueous/nonaqueous liquid or solution with surfactant), the particle size and distribution can be adjusted.[1] Metal nanoparticles such as Ag,[2] Au,[3] and Pt[4] have been fabricated using this method. Recently, this technique was used to fabricate permalloy nanoparticles.[5,6] Permalloy is an important magnetic material with potential applications in catalysis,[7] biomedicine,[8] and electronic devices.[9]

Although one can optimize the experimental conditions to achieve desirable nanoparticle sizes, the size distribution of nanoparticles fabricated by laser ablation in liquid is generally broad.[10,11] This is partly due to the fact that previously produced particles may re-enter the laser beam and thus be further processed. Laser fragmentation, i.e., the gradual decrease in the average size of particles upon laser reirradiation, is a phenomenon that has been recognized as an active mechanism during laser ablation of solid targets in liquid.[10,11] Laser irradiation could also induce agglomeration of metal nanoparticles in liquid, for example, the formation of Au networks from nanoparticles due to intense pulsed laser irradiation.[12] However, no constructive processes, namely, laser-induced assembly and coalescence of metal particles, have been reported previously.

Herein, we show how unique micro/nanostructures, especially fullerene-like hollow microparticles assembled from permalloy particles with diameters of 400−600 nm, can be generated by pulsed excimer laser ablation of a permalloy target in sodium dodecyl sulfate (SDS) aqueous solution. These unique microparticles are likely due to competition between laser-induced assembly and fragmentation and between photothermal and quenching in the liquid environment, and due to the laser-produced bubbles accompanying the laser ablation of the target.

2. Experimental Section

In the experiment, a KrF excimer laser (wavelength 248 nm, pulse width 30 ns) was focused onto the surface of a permalloy disk (Kurt J. Lesker, Ni 81 wt %, Fe 19 wt %). The target was placed on the bottom of a rotating glass dish filled with 0.05 M SDS aqueous solution at 5 mm below the solution surface. The laser frequency was 20 Hz, the fluence was 7 J/cm^2, and the irradiation times were between 20 min and 9 h. The resulting particles were subsequently isolated by centrifugation, purified by washing, and redispersed in distilled water and ethanol, respectively, to remove any soluble residues.

The morphology and structure of the products were characterized with a field emission scanning electron microscope (FE-SEM, JEOL JSM-6330F) with energy-dispersive X-ray spectroscopy (EDS) and a transmission electron microscope (TEM, Philip CM12) equipped with selected area electron diffraction (SAED). X-ray diffraction (XRD) patterns were collected on a X-ray diffractometer (Bruker D8) with Cu Kα radiation (λ = 1.5406 Å). Raman spectra were recorded with a Renishaw S2000 Raman spectroscope using an argon-ion laser (514 nm).

3. Results and Discussion

3.1. Ablation for 20 min, Fabrication of Nanoparticles. Figure 1a shows an SEM image of the permalloy particles obtained with ablation time of 20 min. Most of the particles

* Corresponding author. E-mail: Cerasela-Zoica.Dinu@mail.wvu.edu (C.Z.D.); chrisd@rpi.edu (D.B.C.).
[†] Rensselaer Polytechnic Institute.
[‡] Clemson University.
[§] University of Missouri-Kansas City.
[||] U.S. Naval Research Laboratory.
[⊥] West Virginia University.

10.1021/jp911566a
Published on Web 02/15/2010

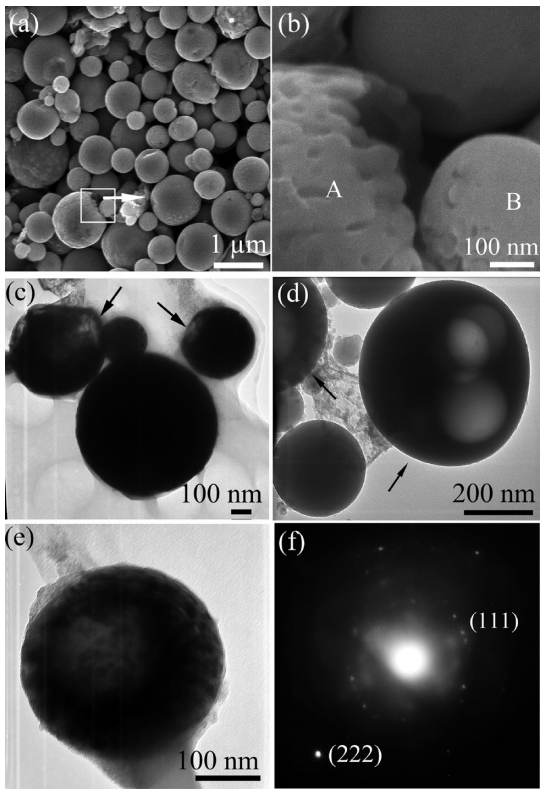

Figure 1. Characterization of permalloy particles produced with ablation time of 20 min: (a) SEM image of the particles; (b) SEM image of a typical particle aggregated by nanoparticles; (c,d) TEM images of the particles with hollow ones denoted by the arrows; (e) TEM image of a particle aggregated by nanoparticles and (f) the corresponding SAED pattern.

are spherical with a distribution in diameters from 300 nm to 1 μm. Some particles seem to be aggregated from nanoparticles (in the region indicated by the arrow). The high-resolution SEM image of two such aggregates (denoted as particles A and B, respectively) is shown in Figure 1b. Examination of particles A and B showed that they were coalesced from nanoparticles with diameters of about 70 nm. A shell-like structure was apparently formed by a layer of nanoparticles as shown by the particle A. We propose that the mechanism leading to the formation of the shell-like structure is due to laser sintering. Specifically, particle B in Figure 1b has a double-featured surface topography with a smooth side and a rough side, respectively. This indicates that a temperature gradient occurred during the laser irradiation. The absorbed photon energy is thermalized and subsequently transferred to the particle as heat. Figure 1c−e shows the TEM images of the particles. It should be noted that most of the nanoparticles are solid spheres, but it is interesting to observe that some nanoparticles have a shell structure and are hollow inside. The shells around two nanoparticles in Figure 1c can be clearly seen as indicated by the black arrows. Figure 1d also shows two hollow spheres. The right one indicated by the arrow is very unique since four spherical cavities are involved. Figure 1e shows a spherical permalloy particle with diameter of about 300 nm that is densely populated by smaller nanoparticles. Moreover, there is an apparent contrast variation in the center of the particle, suggesting that there is a hollow space within the particle presumably due to insufficient packing of the encapsulated nanoparticles. The SAED of the whole particle is shown in Figure 1f. The diffraction ring indicates that the particle is polycrystalline while the encapsulated nanoparticles are not oriented.

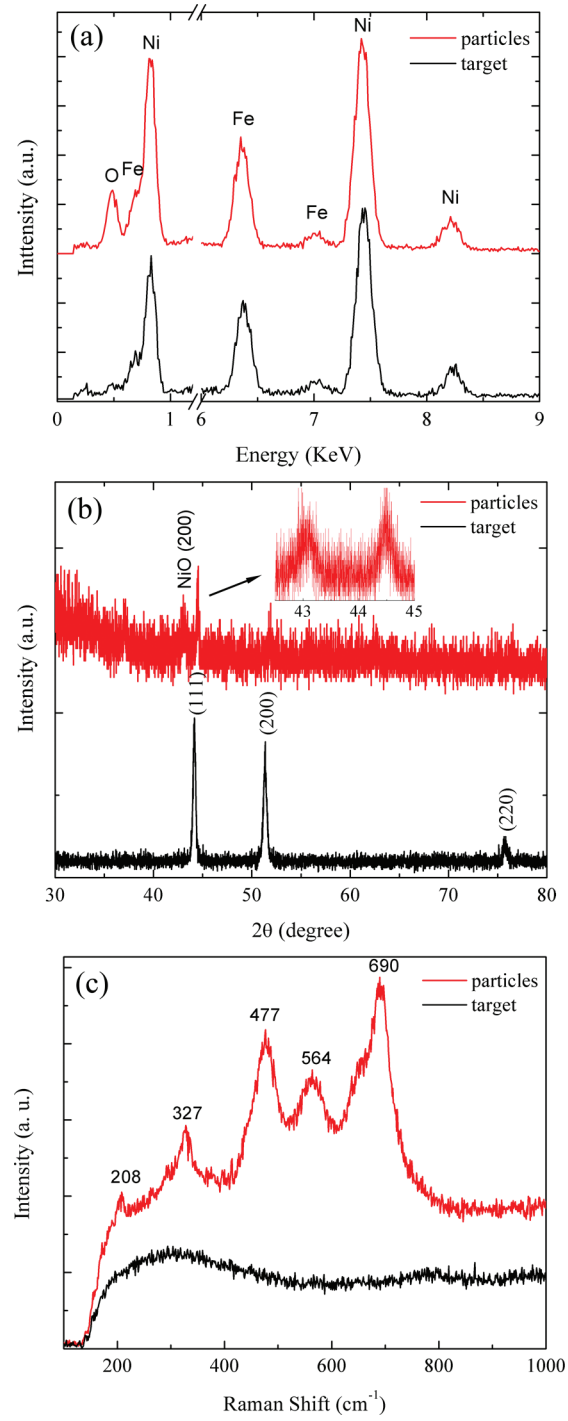

Figure 2. (a) EDS spectra, (b) XRD patterns, and (c) Raman spectra of the permalloy particles and the target.

Figure 2a shows the EDS pattern of the permalloy particles; both Fe and Ni elements were detected, and the composition of Fe and Ni within the particles was close to that of the target. Oxygen was also identified in the spectrum, indicating that the particles were oxidized. No other elements, especially Na or C from the SDS, were detected. The permalloy particles were further studied by XRD. Figure 2b shows the XRD patterns of the target and particles. The target has a face-centered cubic (fcc) structure with $a = 3.55$ Å. The particles have the same structure, but $a = 3.53$ Å and an additional peak is observed at $d = 2.10$ Å, which belongs to NiO (JCPDS file No. 78−0643). This is consistent with the XRD analysis results of permalloy nanoparticles fabricated by pulsed excimer laser ablation in

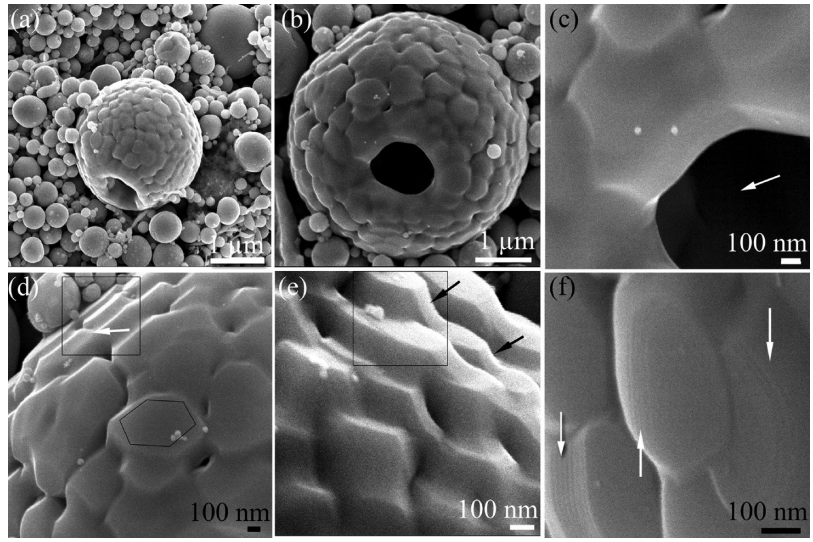

Figure 3. SEM images of permalloy particles produced with ablation time of 4 h: (a,b) typical microparticles assembled from nanoparticles; (c−f) the surface morphologies of the assemblies.

liquid recently.[5] However, study on surface oxidation of permalloy thin films showed that the oxide consisted of a NiO layer on an Fe oxide layer.[13] Thus, we further verified the chemical composition of the oxides in the permalloy particles using Raman spectroscopy. Figure 2c shows the Raman spectra. It can be seen that there are five peaks at 208, 327, 477, 564, and 690 cm^{-1}, respectively. The first two peaks belong to α-Fe_2O_3,[14] the 477 cm^{-1} peak relates to Ni_2O_3[15] and the 564 cm^{-1} belongs to NiO.[16] The peak at 690 cm^{-1} is a character of the first stage oxidation of Fe_3O_4.[17] Thus we can see that the permalloy nanoparticles contain complex oxides, although the XRD pattern mainly shows a NiO peak.

3.2. Ablation for 4 h, Laser-Induced Assembly and Sintering. When the ablation time was increased to 4 h, we observed that some of the particles had assembled into fullerene-like hollow structures as shown in Figure 3a,b. Figure 3c−f represents the high magnification of the surface morphology of the assemblies. Several features are identified:

(i) Holes with diameters of about 1 μm are identified on their surfaces, indicating the formation of hollow structures. A magnified hole is shown in Figure 3c. Around the hole, the particles have totally coalesced together while the morphology of those far from the hole is being individually identified.

(ii) The surface of each assembly is formed from closely packed particles with similar sizes (typically 400−600 nm). These particles are polyhedral, while some local areas are constructed by parallel facets (the square areas in Figure 3d,e).

The polyhedral structure of the assembled particles is the best confirmation of the surface sintering mechanism. The flat faces of particles are the planar facets according to the Wulff construction, which is formed by minimizing surface energy for a given volume and depicts the equilibrium shape of a bulk crystal.[18] In the classic sintering model, spherical powders adopt the shape of a tetrakaidecahedron determined by the Wulff construction.[19] For an fcc structure as the one identified in Figure 1e, it is established by truncating symmetrically six vertices of a octahedron with six square (100) and eight hexagonal (111) facets at its surface.[18] The hexagonal facets can be seen in Figure 3d. These parallel facets build up a sequence of steps identified in Figure 3d,e by the arrows; the height of each step is up to 100 nm. The steps seem to be connected by sloped surfaces constructed from a series of ledges. Typical ledges with height of about 10 nm can be observed in Figure 3f. Such unique structure indicates that the (111) facets are laterally growing. One may expect that the further growth and overlapping of these facets would induce a smooth surface. To confirm this, we increased the ablation time to 9 h, and assembled particles within different sintering stages have been observed.

Figure 4a−e exhibits five such assemblies. In the initial stage of the laser sintering (panels a, b, and g, which is a magnified surface image), the interparticle necking growth was achieved by the repeated pulsing of the laser. In the intermediate stage (panel c and the magnified surface shown in panel f), the (111) facets laterally grow and additional sintering occurs. Finally, spherical particles with shell-like structures were formed (panels d and e).

3.3. Ablation of 9 h, Laser Fragmentation. It is important to note that although increasing the ablation time to 9 h could induce complete sintering of some assemblies, the main products were small nanoparticles. Figure 5a shows the SEM image of the products. Although the products contained a number of assemblies as indicated by the arrows, the majority are nanoparticles as shown in Figure 5b. TEM analysis shows that the diameters of the NPs are about 40−60 nm as shown in Figure 5c. The corresponding SAED patterns of several particles can be calculated and indexed to the (111), (200), (220), and (311) planes with an fcc structure.

The formation of these nanoparticles is mainly due to the laser fragmentation, which is active during laser ablation in liquid. The fragmentation is probably due to charging of the parent particles under laser irradiation and explosive breaking up after accumulating sufficient charge through the photoelectron emission.[20] The Fe and Ni work function is 4.5 and 5.2 eV, respectively. Under the 5 eV excimer laser irradiation, photoemission of electrons could occur as a result of monophonic or multiphoton ionization. But when the ablation time is not so long, the particle concentration in the liquid is low, resulting in a low possibility of laser-particle interactions. When the particle concentration increases with the ablation time, the light absorption and scattering by the particles also increases, and the particles are fragmentized into smaller particles. Since smaller particles have higher surface-to-volume ratio, the light absorption and scattering will be enhanced and eventually laser fragmentation of the particles rather than laser ablation of the target dominates the energy consumption. We could make an estimate here. Assume that the amount of permalloy particles

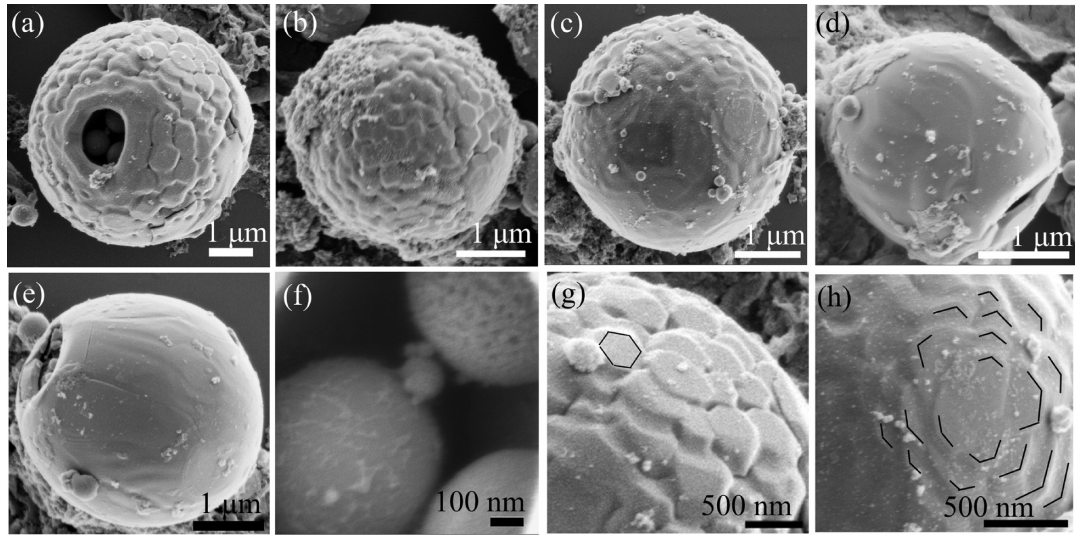

Figure 4. (a−e) SEM images of assemblies showing a typical surface sintering process; (f,g) magnified images of the assemblies in panel a; (h) magnified images of the assemblies in panel c.

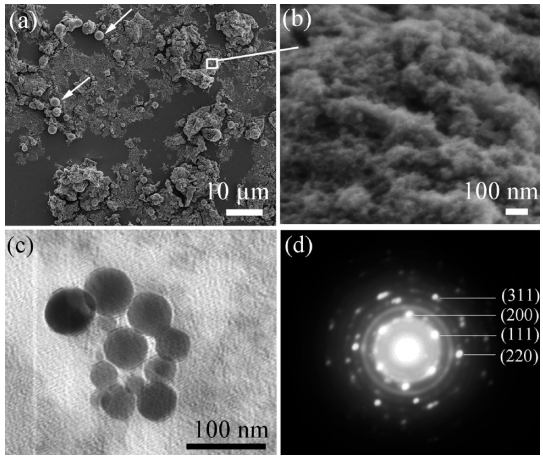

Figure 5. (a) SEM image of permalloy particles produced with ablation time of 9 h; the arrows indicate microparticles assembled from nanoparticles. (b) SEM image of small nanoparticles. (c) TEM image of the nanoparticles and (d) the corresponding SAED pattern.

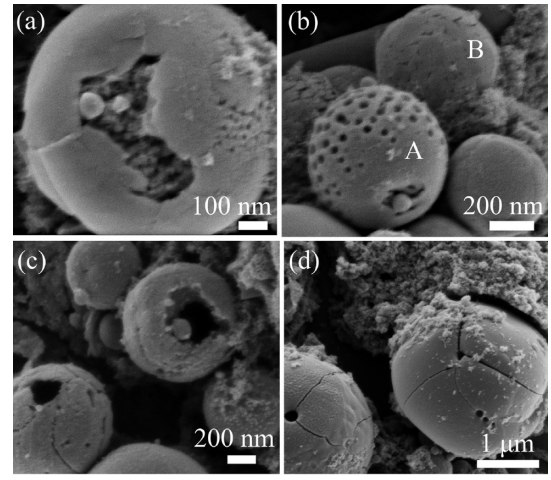

Figure 6. SEM images of permalloy particles with ablation time of 9 h: (a) a cracked nanoparticle in which small nanoparticles are exhibited, (b) nanoparticles with different surface morphologies, (c) cracked hollow nanoparticles, and (d) cracked microparticles.

in the liquid achieves 1 mg and the diameters of the particles are 500 nm. The total cross-sectional area of the particles within the path of a 1 mm^2 laser beam in the liquid is 0.17 mm^2, thus most light could still reach the target. However, if the diameters of the particles reduce to 50 nm, the total cross-sectional area of the particles within the beam path would be 1.7 mm^2, resulting in strong light absorption and scattering and thus laser fragmentation. However, the laser-induced assembly and sintering would still exist for the nanoparticles, which built a dynamic competition with the fragmentation. In Figure 6a, a cracked aggregate is shown. The inside nanoparticles with sizes equal to those of the dispersed nanoparticles can be clearly observed, but the nanoparticles are packaged by a shell due to the surface sintering. The sintering can be also seen in the particles A and B shown in Figure 6b. The pits on them should be the pores before the complete sintering of adjacent surface nanoparticles. The holes or pits on the surface will cause stress concentration during the fragmentation, promoting crack initiation and propagation. These phenomena can be seen in Figure 6c,d, in which cracks propagate along holes on the particle surfaces.

3.4. Mechanism of Assembly. Recent research on laser-induced agglomeration of Au nanoparticles in liquid considered that some of them are negatively charged as a result of surface oxidation followed by deprotonation, while others are positively charged due to electron ejection and Coulombic explosion.[12] As a result, the positively and negatively charged nanoparticles will interact and aggregate.[11] These previously observed mechanisms may provide the explanation for the assembly phenomena of permalloy particles shown in this study. The permalloy particles are also oxidized as indicated by the EDS and XRD analyses. And positive charging due to photoemission has been considered as the reason for laser fragmentation. Thus, both positively and negatively charged particles could be present. But the mechanism responsible for the spherical hollow structure assembly requires greater explanation. Here we consider that the assembly is assisted by the laser-induced bubbles in the liquid. The bubbles came from laser-induced cavitation at the solid−liquid interface.[21] One hypothesis is that the hollow particles shown in Figure 1d were just formed on the bubbles. The bubble interfaces could serve as soft templates for assembly. We noticed that the fullerene-like hollow assembly generally has a hole on the surface and around the hole the nanoparticles have almost coalesced together. Several mechanisms could be proposed for the formation of such holes. First, the hole may

be caused by a shock wave, emanating from the collapse of the template bubble. Secondly, the hole may be formed as a result of the laser ablation of the assembly situated at the most intense regions near the focus of laser beam. However, considering that the size of the hole is much smaller than the laser focal spot, this reason is less possible. Thirdly, the hole may be due to local explosion when the assembly is strongly charged, namely, a process similar to the laser fragmentation. One may wonder that whether the assembly could be induced by magnetic interactions, since permalloy is a ferromagnetic material and the nanoparticles should have interparticle magnetostatic interactions. However, both numerical and experimental investigations have shown that permalloy nanospheres would form a chain-of-sphere structure in favor of lower system energy.[22,23] Nevertheless, the structural order of the final aggregates also indicates a magnetic order, thus further investigation of the synergistic effects of the aggregates would be an interesting topic.

3.5. Thermal Diffusion Length of Laser Sintering and Its Application. Finally we estimate the thermal diffusion length using data of bulk Ni. The thermal diffusion length l_{th} due to laser heating is estimated by

$$l_{th} = (\alpha\tau)^{1/2} \quad (1)$$

where α is the thermal diffusivity and τ stands for the pulse width (30 ns) of the laser,

$$\alpha = k/\rho c_p \quad (2)$$

where k is thermal conductivity, ρ is the density, and c_p is the specific heat capacity. Both k and c_p depend on the temperature of the substance. Considering laser sintering, we assume the temperature is $0.7T_m$ (T_m = melting point of Ni), that is, 1208.2 K. At this temperature, c_p = 1021.42 J/kg·K and k = 64.97 W/m·K,[24] with ρ_{Ni} = 8900 kg/m^2, the thermal diffusion length can be calculated to be 463 nm. However, taking into account that the sintering occurs in a liquid environment, the large thermal conductivity and heat capacity of water on the particle surface will transfer a lot of heat from the particle to the liquid environment.[25] Thus, using the aforementioned bulk material properties for this approximation, the effective laser sintering should only be confined at the particle surface due to the competition of photothermal and quenching effects in the liquid.

Laser surface sintering of metal nanoparticles in liquid may prove to be a more universal approach, because of the unique geometries that are formed. These geometries may find applications in biomedicine for drug delivery, fuel cells for catalysis, and magnetic memory storage. Magnetic nanoparticles can be considered as candidates for drug delivery, but the first requirement is that they should be superparamagnetic.[26] For magnetic nanoparticles, whose bulk counterpart has a remanent moment, the onset of superparamagnetism occurs when the particle diameter is reduced below a critical limit. However, the small size implies a reduced strength of magnetic response, which makes it difficult to direct the nanoparticles to and keep them in the proximity of the target while resisting the drag of blood flow.[26] If the nanoparticles could assemble into larger collections in liquid and then are stabilized by laser surface sintering, the products may synergistically satisfy both the total moment and soft magnetic requirements. That is, the collection of magnetic nanoparticles within the sintered shell can superpose their moment in an external field while retaining their critical diameter individually (remaining superparamagnetic). For this case, and the other aforementioned applications, the new found ability to produce nanoparticle assemblies is especially enabling, and their unique geometries will make unique contributions in disparate applications.

4. Conclusions

Permalloy particles with novel geometries were fabricated by pulsed excimer laser ablation of a permalloy target in SDS aqueous solution. During the ablation process, particles with different morphologies and sizes were obtained as a result of competition between the laser-induced assembly, sintering, and fragmentation of the nanoparticles. Unique fullerene-like hollow microparticles assembled from permalloy particles with diameters of 400−600 nm have been observed in the process. The assembly is assumed to be a result of the electrostatic interactions between charged particles, while the laser-induced bubbles could serve as soft templates for the formation of hollow structures. The laser-induced surface sintering is due to the competition between photothermal and the quenching effects in liquid. Understanding these phenomena will not only benefit the refinement of the laser ablation in liquid, but also provide an approach to fabricate specialized nanostructures.

Acknowledgment. The authors gratefully acknowledge Ray Dove for the instruction on electron microscopy.

References and Notes

(1) Yang, G. W. *Prog. Mater. Sci.* **2007**, *52*, 648.
(2) Mafune, F.; Kohno, J. Y.; Takeda, Y.; Kondow, T.; Sawabe, H. *J. Phys. Chem. B* **2000**, *104*, 9111.
(3) Mafune, F.; Kohno, J. Y.; Takeda, Y.; Kondow, T.; Sawabe, H. *J. Phys. Chem. B* **2001**, *105*, 5114.
(4) Mafune, F.; Kohno, J. Y.; Takeda, Y.; Kondow, T. *J. Phys. Chem. B* **2003**, *107*, 4218.
(5) Musaev, O. R.; Midgley, A. E.; Muthu, D. V. S.; Wrobel, J. M.; Kruger, M. B. *Mater. Lett.* **2009**, *63*, 893.
(6) Bao, R. Q.; Yan, Z. J.; Huang, Y.; Chrisey, D. B. *Mater. Res. Soc. Symp. Proc.* **2008**, *1118*, 1118-K02-08.
(7) Bokare, A. D.; Chikate, R. C.; Rode, C. V.; Paknikar, K. M. *Environ. Sci. Technol.* **2007**, *41*, 7437–7443.
(8) Matthews, B. D.; LaVan, D. A.; Overby, D. R.; Karavitis, J.; Ingber, D. E. *Appl. Phys. Lett.* **2004**, *85*, 2968.
(9) Hytch, M. J.; Dunin-Borkowski, R. E.; Scheinfein, M. R.; Moulin, J.; Duhamel, C.; Mazelayrat, F.; Champion, Y. *Phys. Rev. Lett.* **2003**, *91*, 257207.
(10) Muto, H.; Miyajima, K.; Mafune, F. *J. Phys. Chem. C* **2008**, *112*, 5810.
(11) Werner, D.; Shuichi Hashimoto, S.; Tomita, T.; Matsuo, S.; Makita, Y. *J. Phys. Chem. C* **2008**, *112*, 16801.
(12) Mafune, F.; Kohno, J. Y.; Takeda, Y.; Kondow, T. *J. Phys. Chem. B* **2003**, *107*, 12589.
(13) Fitzsimmons, M. R.; Silva, T. J.; Crawford, T. M. *Phys. Rev. B* **2006**, *73*.
(14) Dagan, G.; Shen, W. M.; Tomkiewicz, M. *J. Electrochem. Soc.* **1992**, *139*, 1855.
(15) Delichere, P.; Joiret, S.; Hugotlegoff, A.; Bange, K.; Hetz, B. *J. Electrochem. Soc.* **1988**, *135*, 1856.
(16) Dietz, R. E.; Parisot, G. I.; Meixner, A. E. *Phys. Rev. B* **1971**, *4*, 2302.
(17) Shebanova, O. N.; Lazor, P. *J. Raman Spectrosc.* **2003**, *34*, 845.
(18) Li, H.; Zhao, M.; Jiang, Q. *J. Phys. Chem. C* **2009**, *113*, 7594.
(19) Coble, R. L. *J. Appl. Phys.* **1961**, *32*, 787.
(20) Kamat, P. V.; Flumiani, M.; Hartland, G. V. *J. Phys. Chem. B* **1998**, *102*, 3123.
(21) Ohl, C. D.; Lindau, O.; Lauterborn, W. *Phys. Rev. Lett.* **1998**, *80*, 393.
(22) Hytch, M. J.; Dunin-Borkowski, R. E.; Scheinfein, M. R.; Moulin, J.; Duhamel, C.; Mazelayrat, F.; Champion, Y. *Phys. Rev. Lett.* **2003**, *91*, 257207.
(23) Ammar, M.; LoBue, M.; Snoeck, E.; Hytch, M.; Champion, Y.; Barrue, R.; Mazaleyrat, F. *J. Magn. Magn. Mater.* **2008**, *320*, e716.
(24) Willis, D. A.; Xu, X. *Int. J. Heat Mass Transfer* **2002**, *45*, 3911.
(25) Shen, M.; Carey, J. E.; Crouch, C. H.; Kandyla, M.; Stone, H. A.; Mazur, E. *Nano Lett.* **2008**, *8*, 2087.
(26) Arruebo, M.; Fernández-Pacheco, R.; Ricardo Ibarra, M.; Santamaría, J. *Nano Today* **2007**, *2* (3), 22.

JP911566A